



Available online at [www.sciencedirect.com](http://www.sciencedirect.com)



ScienceDirect

Trans. Nonferrous Met. Soc. China 26(2016) 1073–1078

Transactions of  
Nonferrous Metals  
Society of China

[www.tnmsc.cn](http://www.tnmsc.cn)



## Quantitative calculation on atomic site occupation during precipitation of Ni<sub>3</sub>(Al<sub>1-x</sub>Fe<sub>x</sub>) by microscopic phase-field study

Hai-hong LIAO, Min-jie LIANG, Pei-kang BAI

School of Materials Science and Engineering, North University of China, Taiyuan 030051, China

Received 8 December 2015; accepted 26 February 2016

**Abstract:** Microscopic phase-field method was used to simulate the site occupation of a series of alloys with a stoichiometric composition of Ni<sub>75</sub>Al<sub>25-x</sub>Fe<sub>x</sub> ( $x=0, 5-10$ ) aged at 1273 K. With the change of Fe content, quantitative calculations were made on each atomic site occupation probability (SOP) in L1<sub>2</sub>-Ni<sub>3</sub> (Al<sub>1-x</sub>Fe<sub>x</sub>), so as to find out the dynamic response law. The result of the study shows that, with the increase of Fe content, the Fe atom preferentially occupies the *B* sites (corner sites of FCC) with its SOP value being increased gradually, and the SOP of the Al atom on the *B* sites is greatly decreased. Meanwhile, Al<sub>Ni</sub> and Fe<sub>Ni</sub> anti-sites form in the precipitation of L1<sub>2</sub> phase. Moreover, with the increase of Fe content, the formation of Al<sub>Ni</sub> and Fe<sub>Ni</sub> anti-sites becomes much easier. In addition, it has been found that the instantaneous dynamic evolution of the atomic SOP is completed at the early stage of the growth of L1<sub>2</sub> phases.

**Key words:** intermetallics; Ni<sub>75</sub>Al<sub>25-x</sub>Fe<sub>x</sub> alloy; atomic site occupation; precipitation; microscopic phase-field

### 1 Introduction

Atomic site occupation behavior in ordered intermetallic compounds is of great practical interest in connection with their high-temperature applications and mechanical properties [1,2]. In particular, Ni<sub>3</sub>Al intermetallic compound with L1<sub>2</sub>-type structure was extensively focused. Various studies have shown that the addition of certain alloying elements can effectively improve its mechanical properties and the effect of the improvement depends on the site occupation of ternary alloying element in Ni<sub>3</sub>Al [3–5]. Thus, the investigation of the atomic site occupation behavior in Ni<sub>3</sub>Al intermetallic compound is extremely useful in controlling and optimizing alloy properties.

Ni<sub>3</sub>Al has L1<sub>2</sub> type face-centered cubic (FCC) structure, in which Ni and Al atoms occupy face-centers (*A* sites) and corners sites (*B* sites) of the FCC unit cell, respectively. However, the site occupation behavior of the different alloying elements in Ni<sub>3</sub>Al exhibits great diversities [4–8]. Fe is one of the most important alloying elements for Ni<sub>3</sub>Al. It can not only improve the ductility and yield strength of alloy, but also drastically affect the electrical and magnetic properties [1,4,6].

Several ways have recently been used to study the site preference of Fe in Ni<sub>3</sub>Al, such as atom probe field-ion microscopy, X-ray diffraction measurement, Mossbauer spectroscopy, the statistical thermodynamic calculation and the first-principles calculations [1,3–9]; however, there are still some controversies about site preference of Fe and the factors affecting site occupation in Ni<sub>3</sub>Al–Fe alloy. For example, IVANOVSKIA et al [4] believed that Fe atoms have preference for Ni sites in nickel deficient Ni<sub>3</sub>Al alloys. NICHOLLS and RAWIINGS [10] have indicated a weak composition-dependent preference for the Al sublattices. SHINDO et al [11] revealed no discernible site preference in Ni<sub>3</sub>Al–Fe system. WU et al [12] showed that site distribution of Fe is a function of the concentration, as well as the matrix composition and temperature. ALMAZOUZI et al [8] indicated that Fe occupies mostly Al sites, regardless of Fe concentration and the matrix composition. By using the Wagner–Schottky model in combination with first-principles calculations, JIANG and GLEESON [13] found that the site preference of Fe strongly depends on the temperature.

The previous investigations were mainly focused on the site preference of Fe. Very limited experimental data about the effects of Fe on atomic site occupation in

**Foundation item:** Project (2013011014-1) supported by the Natural Science Funds of Shanxi Province, China; Project (2009021028) supported by Science and Technique Foundation for Young Scholars of Shanxi Province, China

**Corresponding author:** Hai-hong LIAO; Tel: +86-351-3557392; E-mail: 499257098@qq.com  
DOI: 10.1016/S1003-6326(16)64204-8

$L_{12}\text{-Ni}_3(\text{Al}_{1-x}\text{Fe}_x)$  can be found in the literature and the temporal evolution of atomic site occupation probability (SOP) and anti-site behavior are also not well revealed.

The purpose of the present study is to predict the effect of Fe addition on the atomic SOP during the precipitation process of the  $L_{12}\text{-Ni}_3(\text{Al}_{1-x}\text{Fe}_x)$  with respect to stoichiometric  $\text{Ni}_{75}\text{Al}_{25-x}\text{Fe}_x$  alloy aged at 1273 K. By using the microscopic phase-field model, the temporal evolution of atomic SOP and the anti-sites behavior will be revealed in detail with the varying of Fe content.

## 2 Microscopic phase-field kinetics model

In recent years, phase-field model has been used extensively by the materials scientists. The temporal morphology and the dynamics processes can also be well presented [14–16]. Microscopic phase-field kinetics model was firstly proposed by KHACHATURYAN [17], and is a deterministic phase-field method based on Onsager and Ginzburg–Landau theory. It relates composition to long range order parameter (LRO) by nonequilibrium free energy of atom single-site occupation probability function, and can be used to solve the kinetic equations of ordering and diffusion. Nonhomogeneous system can be simulated with microscopic phase-field kinetics model at atomic-scale, with which, the precipitation caused by atom jumpiness at crystal lattice site can be described [17,18].

Microscopic phase-field dynamic model is used to describe the atomic configurations and phase morphologies by single-site occupation probability functions  $P(\mathbf{r},t)$ , which is the probability that a given lattice site  $\mathbf{r}$  is occupied by an atom at time  $t$ . In this model, the atomic jump is supposed as a direct exchange instead of the vacancy mechanism, and the lattice defects, such as the dislocation, vacancy, are neglected. The change rates of these probabilities are linearly proportional to the thermodynamic driving force [17,18].

$$\frac{\partial P(\mathbf{r},t)}{\partial t} = \sum_{\mathbf{r}'} L(\mathbf{r}-\mathbf{r}') \frac{\delta F}{\delta P(\mathbf{r}',t)} \quad (1)$$

where  $F$  is the total free energy function of  $P(\mathbf{r}',t)$ , and  $L(\mathbf{r}-\mathbf{r}')$  is the symmetry matrix of the microscopic kinetics related to the probability of an elementary diffusion jump from  $\mathbf{r}$  to  $\mathbf{r}'$  per unit of time.

Microscopic diffusion equation of the ternary system was developed by CHEN et al [18,19]. In this model,  $P_A(\mathbf{r},t)$ ,  $P_B(\mathbf{r},t)$  and  $P_C(\mathbf{r},t)$  represent the probabilities of locating an  $A$ ,  $B$  or  $C$  atom, respectively. Since  $P_A(\mathbf{r},t)+P_B(\mathbf{r},t)+xP_C(\mathbf{r},t)=1$ , only two equations are independent at each lattice site. So, the microscopic diffusion equation of ternary system can be obtained. In order to describe the nucleation, a random noise item was added to the right-hand side of the equation, and

then the microscopic Langevin equations become

$$\left\{ \begin{array}{l} \frac{dP_A(\mathbf{r},t)}{dt} = \frac{1}{k_B T} \sum_{\mathbf{r}'} [L_{AA}(\mathbf{r}-\mathbf{r}') \frac{\partial F}{\partial P_A(\mathbf{r}',t)} + \\ L_{AB}(\mathbf{r}-\mathbf{r}') \frac{\partial F}{\partial P_B(\mathbf{r}',t)}] + \xi(\mathbf{r},t) \\ \frac{dP_B(\mathbf{r},t)}{dt} = \frac{1}{k_B T} \sum_{\mathbf{r}'} [L_{BA}(\mathbf{r}-\mathbf{r}') \frac{\partial F}{\partial P_A(\mathbf{r}',t)} + \\ L_{BB}(\mathbf{r}-\mathbf{r}') \frac{\partial F}{\partial P_B(\mathbf{r}',t)}] + \xi(\mathbf{r},t) \end{array} \right. \quad (2)$$

where  $L_{\alpha\beta}(\mathbf{r}-\mathbf{r}')$  is a constant related to the exchange probabilities of a pair of atoms,  $\alpha$  and  $\beta$  ( $= A$ ,  $B$  or  $C$ ), at lattice site  $\mathbf{r}$  and  $\mathbf{r}'$  per unit time,  $\zeta(\mathbf{r},t)$  is the noise term which is taken to be Gaussian-distributed and its correlation properties meet the requirements of the fluctuation dissipation theory,  $k_B$  is the Boltzmann constant, and  $F$  is the total free energy of the system, based on the mean-field approximation [14]:

$$\begin{aligned} F = & -\frac{1}{2} \sum_{\mathbf{r}} \sum_{\mathbf{r}'} [V_{AB}(\mathbf{r}-\mathbf{r}') P_A(\mathbf{r}) P_B(\mathbf{r}') + \\ & V_{BC}(\mathbf{r}-\mathbf{r}') P_B(\mathbf{r}) P_C(\mathbf{r}') + V_{AC}(\mathbf{r}-\mathbf{r}') P_A(\mathbf{r}) P_C(\mathbf{r}') ] + \\ & k_B T \sum_{\mathbf{r}} [P_A(\mathbf{r}) \ln(P_A(\mathbf{r})) + P_B(\mathbf{r}) \ln(P_B(\mathbf{r})) + \\ & P_C(\mathbf{r}) \ln(P_C(\mathbf{r}))] \end{aligned} \quad (3)$$

where  $V_{\alpha\beta}(\mathbf{r}-\mathbf{r}')$  is the interaction energy between  $\alpha$  and  $\beta$  at lattice sites  $\mathbf{r}$  and  $\mathbf{r}'$ .

Substituting Eq. (3) into Eq. (2), Fourier transforming both sides of the kinetic Eq. (2) gives

$$\left\{ \begin{array}{l} \frac{d\tilde{P}_A(\mathbf{k},t)}{dt} = \frac{\tilde{L}_{AA}(\mathbf{k})}{k_B T} \{ \tilde{V}_{AC}(\mathbf{k}) \tilde{P}_A(\mathbf{k},t) + \\ 1/2[-\tilde{V}_{AB}(\mathbf{k}) + \tilde{V}_{BC}(\mathbf{k}) + \tilde{V}_{AC}(\mathbf{k})] \tilde{P}_B(\mathbf{k},t) + \\ k_B T [\ln \frac{P_A(\mathbf{r},t)}{1-P_A(\mathbf{r},t)-P_B(\mathbf{r},t)}]_k \} + \\ \frac{\tilde{L}_{AB}(\mathbf{k})}{k_B T} \{ \tilde{V}_{BC}(\mathbf{k}) \tilde{P}_B(\mathbf{k},t) + 1/2[-\tilde{V}_{AB}(\mathbf{k}) + \\ \tilde{V}_{BC}(\mathbf{k}) + \tilde{V}_{AC}(\mathbf{k})] \tilde{P}_A(\mathbf{k},t) + \\ k_B T [\ln \frac{P_B(\mathbf{r},t)}{1-P_A(\mathbf{r},t)-P_B(\mathbf{r},t)}]_k \} + \xi(\mathbf{k},t) \\ \frac{d\tilde{P}_B(\mathbf{k},t)}{dt} = \frac{\tilde{L}_{BA}(\mathbf{k})}{k_B T} \{ \tilde{V}_{AC}(\mathbf{k}) \tilde{P}_A(\mathbf{k},t) + \\ 1/2[-\tilde{V}_{AB}(\mathbf{k}) + \tilde{V}_{BC}(\mathbf{k}) + \tilde{V}_{AC}(\mathbf{k})] \tilde{P}_B(\mathbf{k},t) + \\ k_B T [\ln \frac{P_A(\mathbf{r},t)}{1-P_A(\mathbf{r},t)-P_B(\mathbf{r},t)}]_k \} + \\ \frac{\tilde{L}_{BB}(\mathbf{k})}{k_B T} \{ \tilde{V}_{BC}(\mathbf{k}) \tilde{P}_B(\mathbf{k},t) + \\ 1/2[-\tilde{V}_{AB}(\mathbf{k}) + \tilde{V}_{BC}(\mathbf{k}) + \tilde{V}_{AC}(\mathbf{k})] \tilde{P}_A(\mathbf{k},t) + \\ k_B T [\ln \frac{P_B(\mathbf{r},t)}{1-P_A(\mathbf{r},t)-P_B(\mathbf{r},t)}]_k \} + \xi(\mathbf{k},t) \end{array} \right. \quad (4)$$

where  $\mathbf{k}$  is the lattice site vector in the reciprocal space,  $\tilde{P}_A(\mathbf{k}, t)$ ,  $\tilde{P}_B(\mathbf{k}, t)$ ,  $\tilde{L}_{AA}(\mathbf{k})$ ,  $\tilde{L}_{AB}(\mathbf{k})$ ,  $\tilde{L}_{BA}(\mathbf{k})$ ,  $\tilde{L}_{BB}(\mathbf{k})$ ,  $\xi(\mathbf{k}, t)$  are Fourier transforms of corresponding functions in the real space.

In this simulation, Eq. (4) is solved by Euler method, and then two-dimensional (2-D) projection of a three-dimensional (3-D) system along the [001] direction is used. Finally, the temporal evolution information of atomic site occupation probability is acquired as a function of the aging time.

### 3 Results and discussion

#### 3.1 Temporal evolution of atomic site occupation probability

Figure 1 shows the temporal evolution of atomic SOP on  $A$  and  $B$  sites in  $L1_2$  phase with the increase of Fe content. At the content of 0 Fe ( $x_{Fe}$ ), before 2000 time steps, the alloy system is disordered; this stage is the incubation period of precipitation, thus the SOP of Al atoms on  $A$  and  $B$  sites are identical on all sites. The incubation period is followed by an ordering process, i.e., the SOP of Al atoms on  $B$  sites starts to increase quickly, and reaches the maximum at the 5500 time steps

(Fig. 1(a)). On the contrary, their SOP on  $A$  sites decreases quickly to the minimum (0.007) and then keeps unchanged (Fig. 1(c)), which indicates Al atoms almost fully occupy  $B$  sites. However, with increasing Fe content, the SOP of Al atoms on  $B$  sites obviously decreases and the atomic ordering is obviously postponed. In the meanwhile, it is further found that a very small amount of Al atoms begin to occupy Ni sites, indicating that the  $Al_{Ni}$  anti-site behavior occurs. Also,  $Al_{Ni}$  anti-site behavior becomes easier and easier with the addition of Fe. Furthermore, it is found that Fe atoms prefer to occupy  $B$  sites (Fig. 1(b)), and a few of Fe atoms occupy  $A$  sites, exhibiting the anti-site behavior (Fig. 1(d)), and their SOP gradually rises not only on  $B$  sites but also on  $A$  sites. The results of the atomic SOP in  $L1_2-Ni_3(Al_{1-x}Fe_x)$  with the increase of Fe content at the final equilibrium state, are listed in Table 1.

From Table 1, it can be seen that for the stoichiometric  $Ni_{75}Al_{25-x}Fe_x$  alloy, Fe and Al atoms occupied  $B$  sites in common, whereas the dependence of the anti-site behavior of Al atoms on composition is relatively weak. The anti-site behavior of Fe atoms becomes stronger and stronger with increasing Fe content.

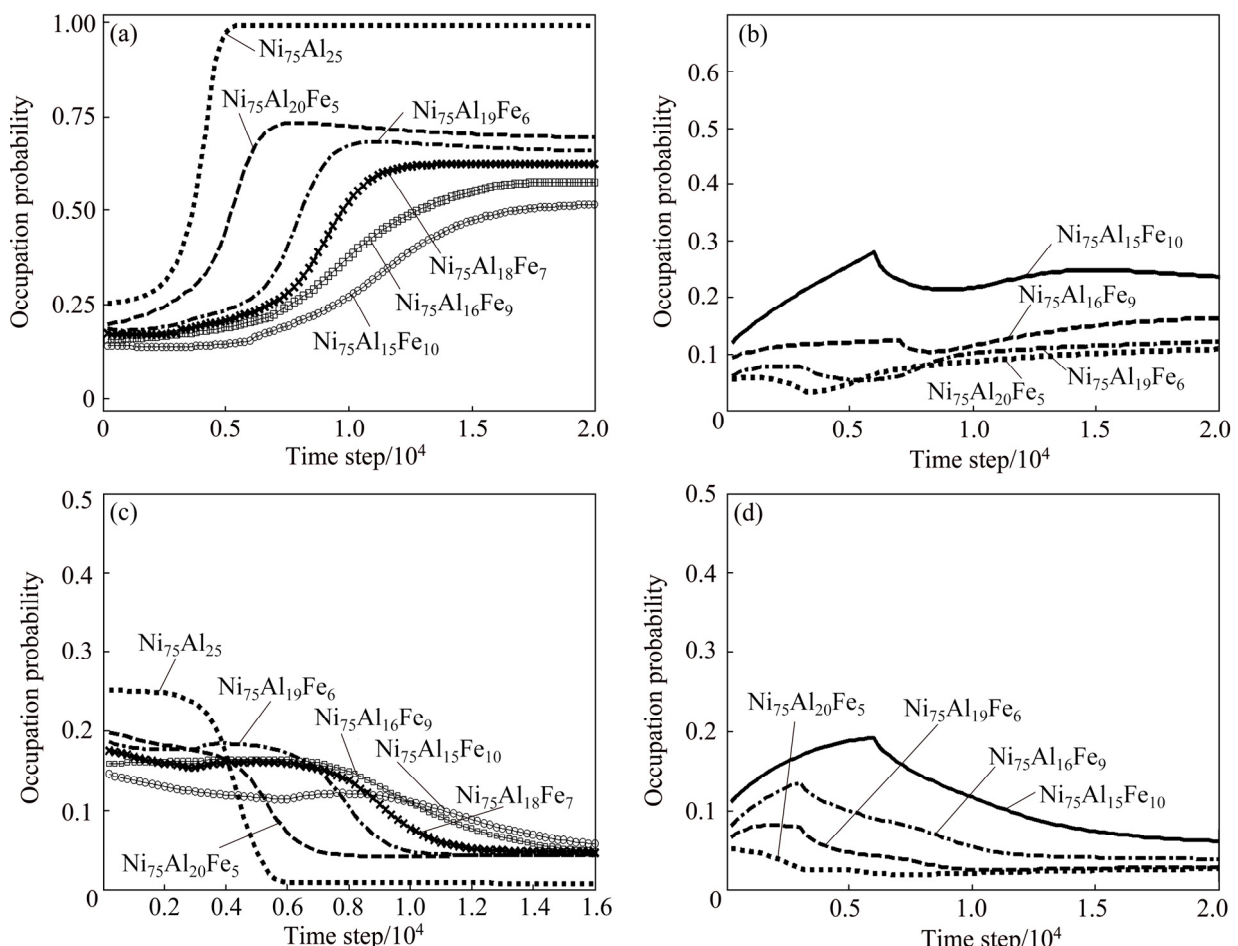


**Fig. 1** Temporal evolution of atomic SOP on  $B$  sites: (a) Al atoms; (b) Fe atoms and on  $A$  sites; (c) Al atoms; (d) Fe atoms in  $L1_2$  phase with increasing Fe content

**Table 1** At equilibrium state, variations laws of atomic site occupation probability in  $L1_2\text{-Ni}_3(\text{Al}_{1-x}\text{Fe}_x)$  with increasing Fe content

Alloy	Occupation probability			
	Al atoms		Fe atoms	
	<i>A</i> sites	<i>B</i> sites	<i>A</i> sites	<i>B</i> sites
$\text{Ni}_{75}\text{Al}_{25}$	0.0079	0.9872	—	—
$\text{Ni}_{75}\text{Al}_{20}\text{Fe}_5$	0.0442	0.6855	0.0285	0.1179
$\text{Ni}_{75}\text{Al}_{19}\text{Fe}_6$	0.0450	0.6451	0.0326	0.1356
$\text{Ni}_{75}\text{Al}_{18}\text{Fe}_7$	0.0461	0.6115	0.0364	0.1500
$\text{Ni}_{75}\text{Al}_{16}\text{Fe}_9$	0.0473	0.5309	0.0459	0.1838
$\text{Ni}_{75}\text{Al}_{15}\text{Fe}_{10}$	0.0477	0.5122	0.0524	0.2087

### 3.2 Evolution of volume fraction of $L1_2\text{-Ni}_3(\text{Al}_{1-x}\text{Fe}_x)$

Figure 2 displays the variation of the volume fraction of  $L1_2\text{-Ni}_3(\text{Al}_{1-x}\text{Fe}_x)$  as a function of time. For  $x_{\text{Fe}}=0.05\%$  alloy, due to the addition of noise item in high temperature, the incubation period of the precipitation shows a disordering fluctuation before 5000 time steps. Then, the volume fraction of  $L1_2$  phases increases quickly and reaches the maximum at the 15000 time steps, which corresponds to a quick growth stage of  $L1_2$  phases. Within 15000 to 20000 time steps, the volume fraction increases slowly and gradually tends to be equilibrium, which is the coarsening stage of  $L1_2$  phases. From Figs. 1(b) and (d) and Fig. 2, it is noticed that during the incubation period of the precipitation, the SOP of Fe atoms on both *A* and *B* sites is also abnormal which is consistent with the state of the volume fraction. From 5000 to 10000 time step, the SOP of Fe atoms on *B* sites gradually increases, and decreases on *A* sites. At the later stage of the growth of  $L1_2$  phases (10000–15000 time steps), the SOP of Fe atoms on both *A* and *B* sites approaches to the equilibrium, and then keep unchanged. As a result, it shows that the site occupation of Fe atoms is already accomplished before the growth of  $L1_2$  phase finishes. Furthermore, with increasing Fe content, the time of the SOP of Fe atoms arriving at the equilibrium

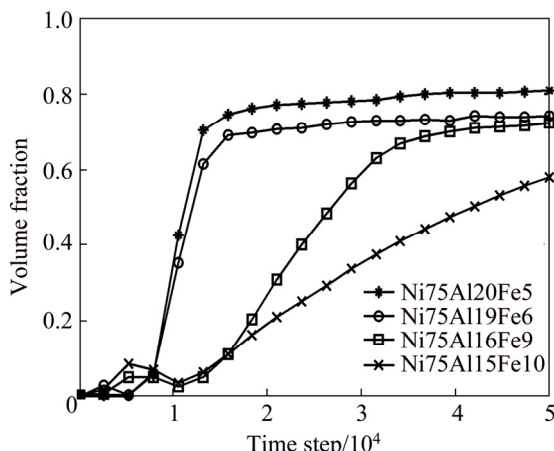


**Fig. 2** Variation of volume fraction with different Fe contents

is much earlier than that of the volume fraction of  $L1_2$  phase, which indicates that the evolution of atomic SOP is already completed at the much earlier stage of the growth of  $L1_2$  phases, and there is almost no change at the later stage of the growth and coarsening stage of  $L1_2$  phases.

### 3.3 Variation of long-range order (LRO) parameter and concentration

Figure 3 shows the variation of LRO parameter and concentration of Al atoms in  $L1_2$  phase with  $x_{\text{Fe}}=0$  and 0.10% alloys. From Fig. 3(a), it can be seen that at 3000 time steps, the LRO parameter shows the larger fluctuation and continuous increase, and then reaches the equilibrium value (about 1) at 4800 time steps. Then, the curves of LRO parameter keep almost unchanged in their height although the width is broadened, which corresponds to the coarsening stage of  $L1_2$  phases. Whereas, at the initial stage of aging, the value of concentration only exhibits smaller fluctuation and slower decrease, and finally reaches the equilibrium value (Fig. 3(b)). From the variation of LRO parameter and concentration curves, it can be indicated that the precipitation mechanism of  $L1_2$  phases has the characteristic of spinodal decomposition.

However, for  $x_{\text{Fe}}=0.10\%$  alloy, the fluctuation of LRO parameter is postponed (Fig. 3(c)), and the equilibrium values of LRO parameter of both Al and Fe atoms in  $L1_2$  phases are significantly decreased, as shown in Fig. 4, which indicates that ordering process of  $L1_2$  phases gradually slackens and their ordering degree obviously descends. Meanwhile, the corresponding concentration curves also present larger fluctuations in the center (Fig. 3(d)). From above analysis, it can be concluded that the formation of  $L1_2$  phases shows more characteristics of non-classical nucleation and growth with increasing Fe content. The addition of Fe obviously changes the precipitation mechanism of  $L1_2$  phases and makes their ordering degree gradually to be decreased.

Some experiments on  $\text{Ni}_3\text{Al}-\text{Fe}$  at 1273 K by SHINDO et al [11] indicated that Fe showed preference on Al sublattices, and the fraction of Fe occupied Al sublattices strongly depended on alloy composition. JIANG and GLEESON [13] also showed that Fe preferred to occupy Al sublattices in Ni-riched  $\text{Ni}_3\text{Al}$  at 1273 K. Further, the atomic anti-site behavior was found in binary  $\text{Ni}_3\text{Al}$  alloy [4,20], which resulted in the formation of Al anti-site defects. From the view of formation enthalpy, JIANG and GLEESON [13] and FU and PAINTER [20] also explained the formation of three structure types of anti-site defects, including  $\text{Al}_{\text{Ni}}$  and  $\text{X}_{\text{Ni}}$  anti-sites. In this work, our simulation results are consistent with the experimental and theoretic results very well.

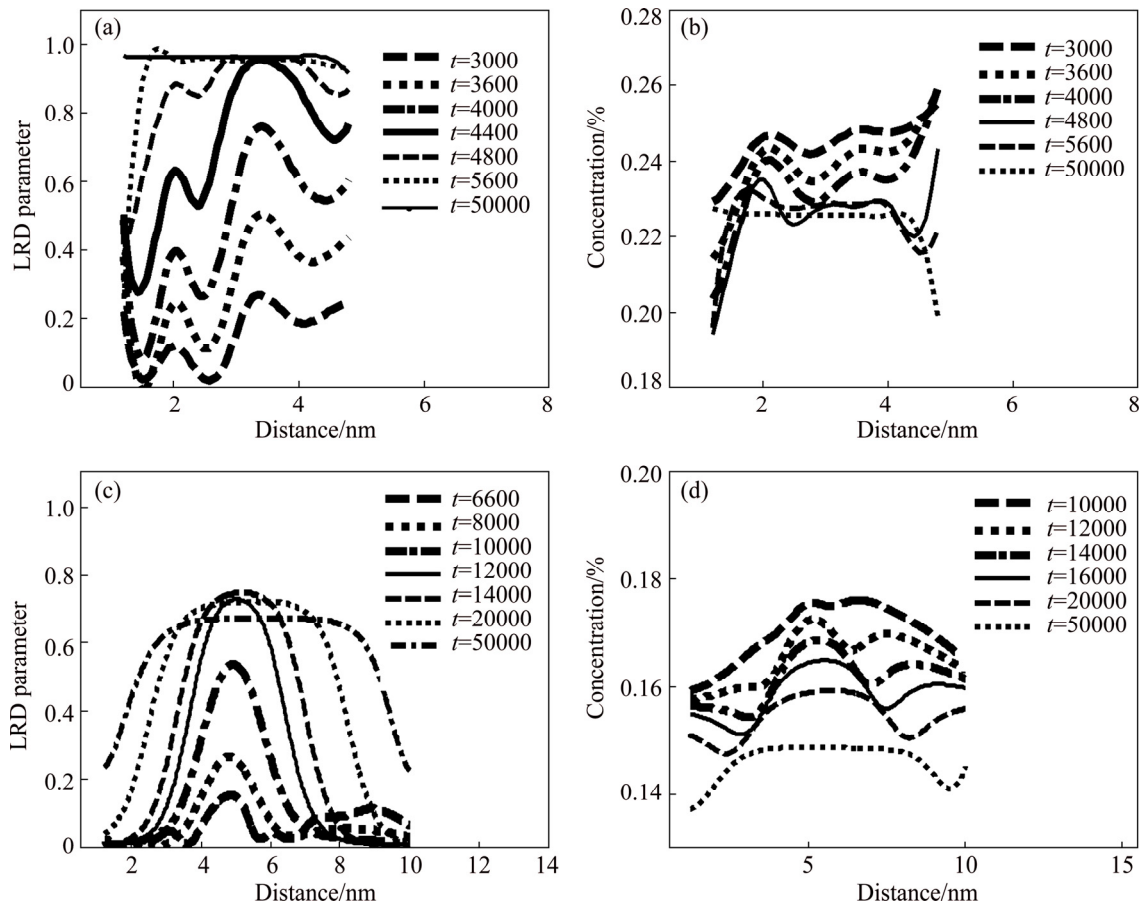


**Fig. 3** LRO and concentration profiles: (a, b)  $\text{Ni}_{75}\text{Al}_{25}$ ; (c, d)  $\text{Ni}_{75}\text{Al}_{15}\text{Fe}_{10}$

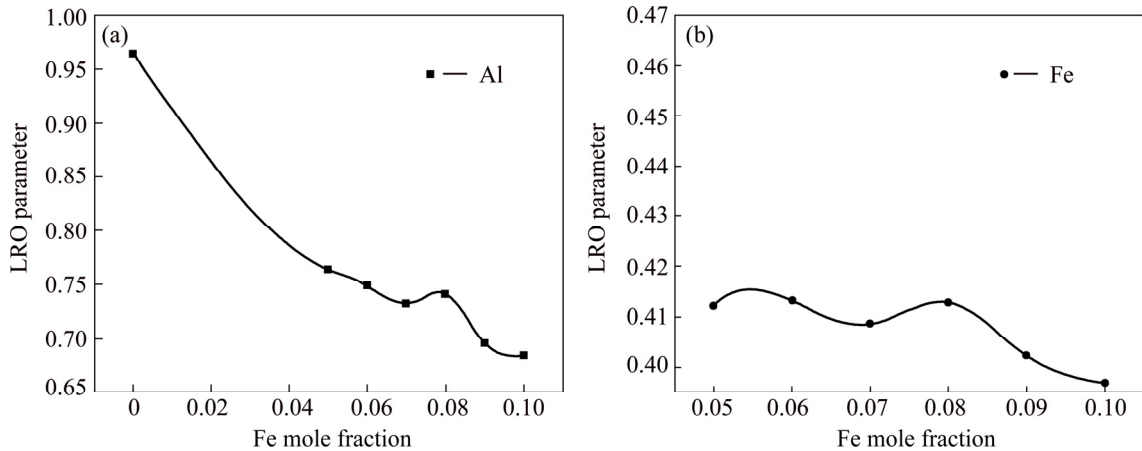


**Fig. 4** Variation of equilibrium value of LRO parameter of Al atoms (a) and Fe atoms (b) in  $\text{L1}_2$  phases with increasing Fe content

## 4 Conclusions

1) In stoichiometric  $\text{Ni}_{75}\text{Al}_{25-x}\text{Fe}_x$  alloy, Fe atoms prefer to occupy *B* sites, so the formed  $\text{L1}_2$  phases are a complex  $\text{Ni}_3(\text{Al}_{1-x}\text{Fe}_x)$ . With the increase of Fe content, the SOP of Fe atoms on *B* sites increases gradually, while the case for Al atoms is opposite.

2) Anti-site behaviors including  $\text{Al}_{\text{Ni}}$  and  $\text{Fe}_{\text{Ni}}$  appear

in precipitation process of  $\text{L1}_2$  phases. Meanwhile, with increasing Fe content,  $\text{Al}_{\text{Ni}}$  and  $\text{Fe}_{\text{Ni}}$  anti-sites all tend to increase, whereas the dependence of  $\text{Al}_{\text{Ni}}$  anti-sites on composition is relatively weak.

3) Evolution of the atomic SOP is already completed at the early stage of the growth of  $\text{L1}_2$  phases, while the SOP almost keeps unchanged at the later stage of the growth and the coarsening of  $\text{L1}_2$  phases.

4) As Fe content increases, the precipitation

mechanism of  $L1_2$ - $Ni_3(Al_{1-x}Fe_x)$  changes from spinodal decomposition to non-classical nucleation and growth. The lower ordering degree of  $L1_2$  phases appears with the continuous increase of Fe content.

## References

- [1] D'SANTHOSHINI B A, KAUL S N. Site preference of ternary Fe addition in  $Ni_{75}Al_{25}$  [J]. *J Phys Condens Matter*, 2003, 15(29): 4903–4918.
- [2] CHANTAL K S, KEVIN E Y, RONALD D N, DAVID N S. Temporal evolution of the nanostructure and phase compositions in a model Ni-Al-Cr alloy [J]. *Acta Materialia*, 2006, 54(12): 3199–3210.
- [3] MOTTURAA A, WARNKENB N, MILLERC M K, FINNIS M W, REED R C. Atom probe tomography analysis of the distribution of rhenium in nickel alloys [J]. *Acta Materialia*, 2010, 58(3): 931–942.
- [4] IVANOVSKI V N, UMIĆEVIĆ A, BELOŠEVIĆ-ČAVOR J, LEI He-chang, LI Li-Jun, CEKIC B, KOTESKI V, PETROVIC C. Local structure study of Fe dopants in Ni-deficit  $Ni_3Al$  alloys[J]. *Journal of Alloys and Compounds*, 2015, 651: 705–711.
- [5] IVANOVSKI V N, CEKIĆ B, UMIĆEVIĆ A, BARUDŽIJA T, SCHUMACHER G, MAĐAREVIĆ I, KOTESKI V. Site preference of Hf dopant in  $Ni_3Al$  alloys: A perturbed angular correlation study [J]. *Journal of Alloys and Compounds*, 2015, 622: 541–547.
- [6] KUMAR A, CHERNATYNSKIY A, HONG M K, PHILLPOT S R, SINNOTT S B. An ab initio investigation of the effect of alloying elements on the elastic properties and magnetic behavior of  $Ni_3Al$  [J]. *Computational Materials Science*, 2015, 101: 39–46.
- [7] LIU Shu-lan, WANG Chong-yu, YU Tao, LIU Zheng-guang. Effect of RE on lattice trapping in  $\gamma'$ - $Ni_3Al$  cracks by atomistic simulation [J]. *Computational Materials Science*, 2015, 97: 102–108.
- [8] ALMAZOUZI A, NUMAKURA H, KOIWA M, HONO K, SAKURAI T. Site occupation preference of Fe in  $Ni_3Al$ : An atom-probe study [J]. *Intermetallics*, 1997, 5(1): 37–43.
- [9] LECHERMANN F, FÄHNLE M, SANCHEZ J M. First-principles investigation of the Ni-Fe-Al system [J]. *Intermetallics*, 2005, 13(10): 1096–1109.
- [10] NICHOLLS J R, RAWLINGS R D. A Mössbauer effect study of  $Ni_3Al$  with iron additions [J]. *Acta Metallurgica*, 1977, 25(2): 187–194.
- [11] SHINDO D, KIKUCHI M, HIRABAYASHI M, HANADA S, IZUMI O. Site determination of Fe, Co and Cr atoms added in  $Ni_3Al$  by electron channelling enhanced microanalysis [J]. *Trans Japan Inst Metals*, 1988, 29(12): 956–961.
- [12] WU Y P, TSO N C, SANCHEZ J M, TIEN J K. Modeling of ternary site occupation in  $L1_2$  ordered intermetallics [J]. *Acta Metallurgica*, 1989, 37(10): 2835–2840.
- [13] JIANG C, GLEESON B. Site preference of transition metal elements in  $Ni_3Al$  [J]. *Scripta Materialia*, 2006, 55(5): 433–436.
- [14] LIANG Min-jie, LIAO Hai-hong, DING Wen-jiang, CHEN Zheng. Microscopic phase-field modeling of atomic anti-site behaviors in precipitation progress of  $Ni_3(AlFe)$  [J]. *Transactions of Nonferrous Metals Society of China*, 2010, 20(10): 1963–1967.
- [15] CHEN L Q. Phase-field models for microstructure evolution [J]. *Annu Rev Mater Res*, 2002, 32(3): 113–140.
- [16] XIAO Rong-zhen, AN Guo-sheng, ZHU Chang-sheng, WANG Zhi-ping, YANG Shi-yin. Comparative analysis of isothermal and non-isothermal solidification of binary alloys using phase-field model [J]. *Transactions of Nonferrous Metals Society of China*, 2014, 24(11): 3639–3644.
- [17] KHACHATURIAN A G. Theory of structural transformations in solids [M]. New York: Wiley, 1983: 139.
- [18] CHEN L Q. Computer simulation of spinodal decomposition in ternary systems [J]. *Acta Metallurgica Materialia*, 1994, 42(10): 3503–3513.
- [19] PODURI R, CHEN L Q. Computer simulation of morphological evolution and coarsening of  $\delta'(Al_3Li)$  precipitates in Al-Li alloys [J]. *Acta Materialia*, 1998, 46(11): 3915–3928.
- [20] FU C L, PAINTER G S. Point defects and the binding energies of boron near defect sites in  $Ni_3Al$ : A first-principles investigation [J]. *Acta Materialia*, 1997, 45(2): 481–488.

## 定量计算 $Ni_3(Al_{1-x}Fe_x)$ 沉淀中原子占位的微观相场研究

廖海洪, 梁敏洁, 白培康

中北大学 材料科学与工程学院, 太原 030051

**摘要:** 采用微观相场方法, 模拟研究了化学计量比为  $Ni_{75}Al_{25-x}Fe_x$ ( $x=0, 5\sim10$ )系列合金在时效温度为 1273 K 时的原子占位情况。通过该方法, 定量计算了  $L1_2$ - $Ni_3(Al_{1-x}Fe_x)$ 沉淀相中各原子的占位几率(SOP), 并获得了其随 Fe 含量变化的动态响应规律。研究结果表明: 随着 Fe 浓度的增加, Fe 原子优先占据 B 格点位置(FCC 结构的角位), 且其原子占位几率数值逐渐增高; Al 原子在 B 格点位置的占位几率则明显降低。同时, 在  $L1_2$  相沉淀过程中出现了  $Al_{Ni}$  和  $Fe_{Ni}$  反位现象; 且随着 Fe 含量的升高,  $Al_{Ni}$  和  $Fe_{Ni}$  原子反位的形成将会变得更加容易。原子占位几率的瞬时动态演化早在  $L1_2$  相长大的初期阶段就已完成。

**关键词:** 金属间化合物;  $Ni_{75}Al_{25-x}Fe_x$  合金; 原子占位; 沉淀; 微观相场

(Edited by Yun-bin HE)